SPATIO-SPECTRAL COLOR FILTER ARRAY DESIGN FOR ENHANCED IMAGE FIDELITY

Keigo Hirakawa and Patrick J. Wolfe

Harvard University
Department of Statistics, School of Engineering and Applied Sciences
Oxford Street, Cambridge, MA 02138 USA
{hirakawa, wolfe}@stat.harvard.edu

ABSTRACT

In digital imaging applications, data are typically obtained via a spatial subsampling procedure implemented as a color filter array—a physical construction whereby only a single color representative is measured at each pixel location. Owing to the growing ubiquity of color imaging and display devices, much recent work has focused on the interplay between color filter array design and subsequent digital processing, including in particular the canonical spatio-chromatic reconstruction task known as demosaicking. Here we consider the problem of improved color filter array design, leading to enhanced image fidelity. We first analyze the limitations of the well-known Bayer pattern, currently most popular in industry. We then propose a framework for designing rectangular color filter arrays amenable to efficient and completely linear reconstruction, and provide examples of new patterns that enable improvements in reconstruction quality.

Index Terms— Image sensors, color measurement, image sampling, image reconstruction, image color analysis

1. INTRODUCTION

Owing to the growing ubiquity of color imaging devices, much recent work has focused on the interplay between their acquisition stages and subsequent digital processing. In most applications, data are obtained via a subsampling procedure implemented as a color filter array (CFA), a physical construction whereby each pixel location measures only a portion of the visible spectrum, selected from amongst a chosen "color partition" of that spectrum—typically corresponding to long, medium, and short wavelengths—which in turn induces a spatial sampling pattern for each such color representative. This array represents one of the first steps in the acquisition pipeline, and hence CFA design determines to a great extent the maximal resolution achievable by subsequent processing schemes. These schemes typically assume a full-color image (i.e., a full set of color triples), and consequently, a key reconstruction task termed *demosaicking* is first necessary. This refers to the inverse problem of reconstructing a spatially undersampled set whose components correspond to particular tristimulus values—typically red, green, and blue.

An ideal demosaicking solution would exhibit two main traits: low computational complexity for efficient hardware implementation, and amenability to analysis for accurate noise suppression. For instance, in the absence of further assumptions on the relationships between tristimulus values, the optimal *linear* reconstruction is indicated by an orthogonal projection onto the space of bandlimited functions, applied separately to each subsampled color channel. However, it is well known that this solution produces unacceptable artifacts, owing to the correlation amongst color components in typical images; witness the large literature on (necessarily nonlinear and heuristic) contemporary demosaicking schemes, as reviewed in [1].

2. COLOR FILTER ARRAY ANALYSIS

To explain the failure of linear reconstruction methods in the demosaicking context, it is helpful to analyze the spatio-spectral properties of typical color images and the Fourier representations that CFA samplings induce. The most well known of these patterns involve the canonical tristimulus values of red, green, and blue; in particular, the popular Bayer pattern CFA [2] attempts to complement humans' spatial color sensitivity via a quincunx sampling of the green component that is twice as dense as that of red and blue (see Figure 3(a)). Though the Bayer pattern remains the industry standard, a number of alternative color partitions and geometries have been considered over the years—several of which are reviewed in [3].

In each case the regular, repeating CFA pattern comprises a tiling of the image plane formed by the the union of interleaved sampling lattices [4]; such representations are most easily analyzed according to their lattice structure [5]. While space limitations preclude an extended discussion, we remind the reader that lattices constitute a discrete Abelian group under addition, and hence admit as their Fourier transform a so-called dual lattice. The spectral periodicity properties of a color image sampled along a lattice are determined by this dual lattice (the Poisson summation formula being a simple univariate example), thereby enabling us to characterize the effect on individual color channels of the spatio-spectral sampling induced by various CFA patterns. According to the discrete and periodic nature of these patterns, the dual lattice defines a unit cell whose copies in turn form a tessellation of the spatial frequency plane.

To make this notion precise, let $\boldsymbol{n} \in \mathbb{Z}^2$ index pixel location, and denote the corresponding color triple $\boldsymbol{x}(\boldsymbol{n}) = (\boldsymbol{r}(\boldsymbol{n}), \boldsymbol{g}(\boldsymbol{n}), \boldsymbol{b}(\boldsymbol{n}))$. The Bayer pattern, as well as others that attempt to measure tristimulus values, can then be represented conceptually in terms of a green channel $\boldsymbol{g}$ and two difference channels $\boldsymbol{\alpha} = \boldsymbol{r} - \boldsymbol{g}$ and $\boldsymbol{\beta} = \boldsymbol{b} - \boldsymbol{g}$, whose Fourier transforms will be denoted respectively by $\boldsymbol{G} = \mathcal{F}(\boldsymbol{g})$, $\boldsymbol{A} = \mathcal{F}(\boldsymbol{\alpha})$, and $\boldsymbol{B} = \mathcal{F}(\boldsymbol{\beta})$. The advantage of this representation, as noted by [4, 6], is that these difference images can serve as a proxy for chrominance, whereas the green channel can be taken to represent luminance. It is known how to explicitly compute the spectral representation induced by the spatial subsampling of a particular CFA pattern; for the case of the Bayer pattern, see [4, 6, 7].

Because the spatio-spectral content of color channels tends to be correlated at high spatial frequencies [1, 8], the difference channels $\boldsymbol{\alpha}(\boldsymbol{n})$ and $\boldsymbol{\beta}(\boldsymbol{n})$ typically occupy less bandwidth than the green channel $\boldsymbol{g}(\boldsymbol{n})$, as shown in Figure 1 overleaf. This correlation explains in large part the poor performance of naive linear reconstruction attempts, and is exploited (either implicitly or explicitly) in most contemporary Bayer-pattern demosaicking methods [3]. In fact, as shown in [4, 6], the subsampling lattices which comprise the Bayer pattern induce spectral copies of the difference signals centered about the set of carrier frequencies $\{(0, \pi), (\pi, 0), (\pi, \pi)\}$ (see

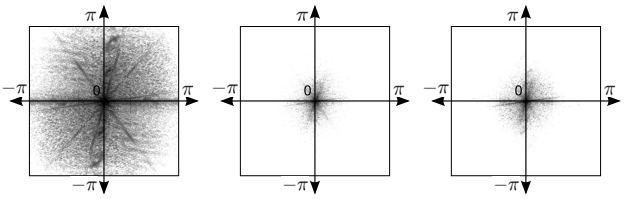

(a) Green spectrum $\boldsymbol{G}$ (b) Difference $\boldsymbol{A}(\boldsymbol{\omega})$ (c) Difference $\boldsymbol{B}(\boldsymbol{\omega})$

Fig. 1. Log-magnitude spectra of a typical color image ("lighthouse"), showing: (a) $\boldsymbol{g}(\boldsymbol{n})$ component, (b) difference image $\boldsymbol{\alpha}(\boldsymbol{n}) = \boldsymbol{r}(\boldsymbol{n}) - \boldsymbol{g}(\boldsymbol{n})$, (c) difference image $\boldsymbol{\beta}(\boldsymbol{n}) = \boldsymbol{b}(\boldsymbol{n}) - \boldsymbol{g}(\boldsymbol{n})$.

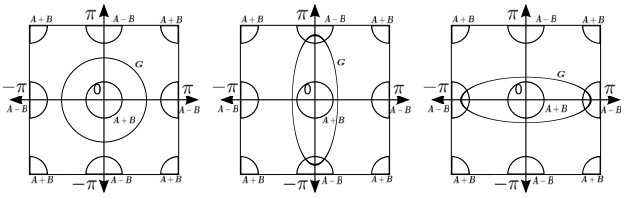

(a) Radially symmetric (b) Horizontal feature (c) Vertical feature

Fig. 2. (a) Idealized spectrum of Bayer pattern sensor image, with spectral replication of $\boldsymbol{A}$ and $\boldsymbol{B}$ about $\{(0,\pi),(\pi,0),(\pi,\pi)\}$. (b) Locally horizontal image feature. (c) Locally vertical image feature. To simplify notation, multiplicative constants have been omitted.

Figure 2). Hence, by reducing allowable spectral bandwidth along these axes, the Bayer spectral periodization (as well as that of others reviewed in [3]) is sensitive to the very horizontal and vertical features which frequently dominate typical images [9].

Figures 2(b) and 2(c) indicate these scenarios, respectively; it may be seen that in contrast to the radially symmetric baseband spectrum of Figure 2(a), aliasing occurs along one of either the horizontal or vertical axes with respect to $\boldsymbol{\alpha} - \boldsymbol{\beta}$. However, successful reconstruction can still occur if the non-corrupted copy of $\boldsymbol{\alpha} - \boldsymbol{\beta}$ is recovered, thereby explaining the popularity of (nonlinear) directional filtering steps [3, 4, 7]. We can therefore view the CFA design problem as one of spatial-frequency multiplexing, and the CFA demosaicking problem as one of demultiplexing to recover subcarriers, with spectral aliasing given the interpretation of "cross talk" [4].

3. COLOR FILTER ARRAY DESIGN

Having identified several obstacles presented by the Bayer pattern itself, we now move to consider the more fundamental question of CFA *design*. Assuming a regular, repeating rectangular pattern, and putting aside issues of white-balancing and sensor noise, the analysis above motivates us to consider *linear combinations* of the Bayer pattern filters. Considering convex combinations of "prototype" filter specifications $\{\boldsymbol{c}_r, \boldsymbol{c}_g, \boldsymbol{c}_b\}$, we are left with three design parameters: the number of distinct color filters, their specifications in terms of linear combinations, and the geometry of the chosen CFA pattern.

To wit, let $0 \leq \boldsymbol{c}_r(\boldsymbol{n}), \boldsymbol{c}_g(\boldsymbol{n}), \boldsymbol{c}_b(\boldsymbol{n}) \leq 1$, with $\boldsymbol{c}_g(\boldsymbol{n}) = 1 - \boldsymbol{c}_r(\boldsymbol{n}) - \boldsymbol{c}_b(\boldsymbol{n})$, represent the CFA projection values at a particular spatial location. Then at pixel location $\boldsymbol{n}$, the image sensor measures a *mixture* of prototype channels according to $\boldsymbol{y}(\boldsymbol{n})$ as follows [10]:

$$\begin{aligned}\boldsymbol{y}(\boldsymbol{n}) =& \boldsymbol{g}(\boldsymbol{n})\boldsymbol{c}_g(\boldsymbol{n}) + \boldsymbol{r}(\boldsymbol{n})\boldsymbol{c}_r(\boldsymbol{n}) + \boldsymbol{b}(\boldsymbol{n})\boldsymbol{c}_b(\boldsymbol{n}) \\ =& \boldsymbol{g}(\boldsymbol{n}) + \boldsymbol{c}_r(\boldsymbol{n})\left[\boldsymbol{r}(\boldsymbol{n}) - \boldsymbol{g}(\boldsymbol{n})\right] + \boldsymbol{c}_b(\boldsymbol{n})\left[\boldsymbol{b}(\boldsymbol{n}) - \boldsymbol{g}(\boldsymbol{n})\right] \\ =& \boldsymbol{g}(\boldsymbol{n}) + \boldsymbol{c}_r(\boldsymbol{n})\boldsymbol{\alpha}(\boldsymbol{n}) + \boldsymbol{c}_b(\boldsymbol{n})\boldsymbol{\beta}(\boldsymbol{n}).\end{aligned} \tag{1}$$

Recalling the lowpass properties of $\boldsymbol{\alpha}(\boldsymbol{n})$ and $\boldsymbol{\beta}(\boldsymbol{n})$, we see that our formulation of the CFA design problem enables us to *modulate* these terms via multiplication with $\boldsymbol{c}_r(\boldsymbol{n})$ and $\boldsymbol{c}_b(\boldsymbol{n})$, such that the Fourier transforms of the frequency-modulated difference images are *maximally separated* from the baseband spectrum of $\boldsymbol{g}(\boldsymbol{n})$. To accomplish this task, let us assume that the Fourier transforms of $\boldsymbol{c}_r$ and $\boldsymbol{c}_b$, respectively, take the form

$$\begin{cases}\mathcal{F}(\boldsymbol{c}_r) = s_0\delta(\boldsymbol{\omega}) + \sum_{i,i\neq 0}\left[s_i\delta(\boldsymbol{\omega}+\boldsymbol{\omega}_i) + \bar{s}_i\delta(\boldsymbol{\omega}-\boldsymbol{\omega}_i)\right] \\ \mathcal{F}(\boldsymbol{c}_b) = t_0\delta(\boldsymbol{\omega}) + \sum_{i,i\neq 0}\left[t_i\delta(\boldsymbol{\omega}+\boldsymbol{\omega}_i) + \bar{t}_i\delta(\boldsymbol{\omega}-\boldsymbol{\omega}_i)\right]\end{cases},$$

where $\bar{\cdot}$ denotes complex conjugation; symmetry ensures that the resultant $\boldsymbol{c}_r, \boldsymbol{c}_b$ are real valued. It follows that the Fourier transforms of products $\boldsymbol{c}_r(\boldsymbol{n})\boldsymbol{\alpha}(\boldsymbol{n})$ and $\boldsymbol{c}_b(\boldsymbol{n})\boldsymbol{\beta}(\boldsymbol{n})$ are the sums of modulated difference images, and hence that of the observed sensor image $\boldsymbol{y}$ is

$$\begin{aligned}\mathcal{F}(\boldsymbol{y}) = \mathcal{F}(\boldsymbol{g} + \boldsymbol{c}_r\boldsymbol{\alpha} + \boldsymbol{c}_b\boldsymbol{\beta}) = \boldsymbol{G}(\boldsymbol{\omega}) + s_0\boldsymbol{A}(\boldsymbol{\omega}) + t_0\boldsymbol{B}(\boldsymbol{\omega}) \\ + \sum_{i,i\neq 0}\left[(s_i\boldsymbol{A} + t_i\boldsymbol{B})(\boldsymbol{\omega}+\boldsymbol{\omega}_i) + (\bar{s}_i\boldsymbol{A} + \bar{t}_i\boldsymbol{B})(\boldsymbol{\omega}-\boldsymbol{\omega}_i)\right].\end{aligned}$$

This approach enables the specification of CFA design parameters directly in the Fourier domain, by way of carrier frequencies $\{\boldsymbol{\omega}_i\}$ and weights $\{s_i, t_i\}$; determination of the resultant color filters and lattice geometry follows by inverse Fourier transform. Hence, we may aim to design CFA patterns such that the spectrum $\mathcal{F}(\boldsymbol{y})$ of the observed sensor image $\boldsymbol{y}$ can be mapped to a baseband component $\boldsymbol{G} + s_0\boldsymbol{A} + t_0\boldsymbol{B}$ and modulated signals $s_i\boldsymbol{A} + t_i\boldsymbol{B}$ and $\bar{s}_i\boldsymbol{A} + \bar{t}_i\boldsymbol{B}$ in such a way as to *minimize* spectral overlap.

Taking the Bayer representation shown in Figure 2 as a motivating example, we see that carrier frequencies should be restricted to the *perimeter* of the unit cell of the CFA's dual lattice, but moved *away* from the frequency axis intercepts $(0,\pi)$ and $(\pi,0)$ in order to maximize the allowable alias-free spectral radii of the baseband and modulated components. Note that we assume a worst-case radial symmetry independent of the edge orientations of any particular image; however, we can expect to see even greater performance improvements in images where horizontal and vertical edges dominate. Constraining carrier frequencies to be rational multiples of π will ensure periodicity of the resultant CFA pattern, and nonnegativity of $\boldsymbol{c}_r(\boldsymbol{n})$ and $\boldsymbol{c}_b(\boldsymbol{n})$ (necessary for physical realizability) is ensured by setting DC coefficients s_0 and t_0 sufficiently large to outweigh the negative pixel-domain values introduced by $\{s_i, t_i\}$ for $i \neq 0$. The size of the weights $\{s_i, t_i\}$ for $i \neq 0$ will in turn will affect robustness to any worst-case chrominance-on-luminance aliasing that might occur, and thus should be chosen to be as large as possible within the constraint of physical realizability described above.

4. EXAMPLE PATTERNS AND RECONSTRUCTIONS

The criteria outlined above provide a clear set of guidelines for spatio-spectral CFA design; once a pattern size has been selected, numerical optimization schemes may be used to generate admissible patterns. To this end we provide three example patterns designed "by hand" to yield closed-form expressions, as shown in Figures 3(b)–3(d) and Table 1. While these patterns are each distinct from the Bayer pattern in color and geometry, their pixels all maintain equal numbers of adjacent colors—an important consideration in minimizing the effects of optical and electrical cross talk between neighboring pixels [3].

To investigate the efficacy of these example patterns and their corresponding linear demosaicking schemes, a standard test set of twenty digital Kodak images originally acquired on film [8] was used to provide full-color proxy data for purposes of comparison to existing algorithms. In keeping with standard practice in the literature,

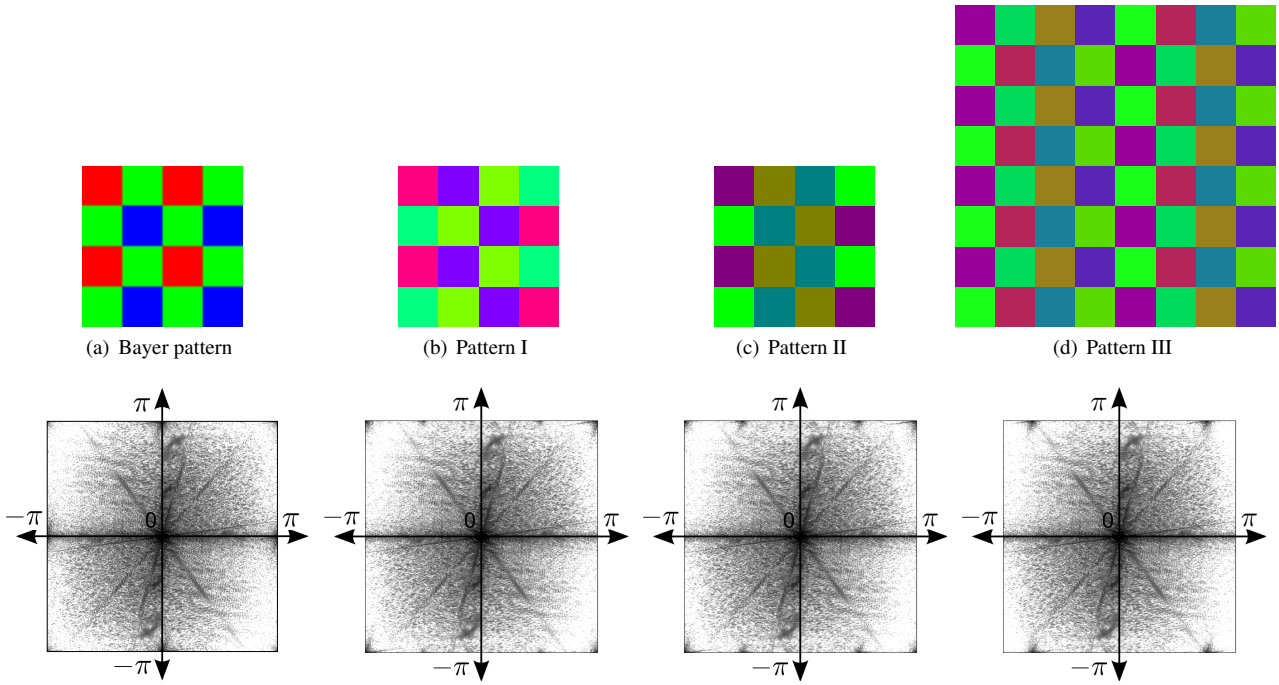

Fig. 3. New CFA designs evaluated in the experiments of Section 4 (top row): (a) Bayer pattern, (b) pattern I, (c) pattern II, (d) pattern III. Respective log-magnitude spectra of sensor images representing the "lighthouse" test image are shown in the bottom row (e–h).

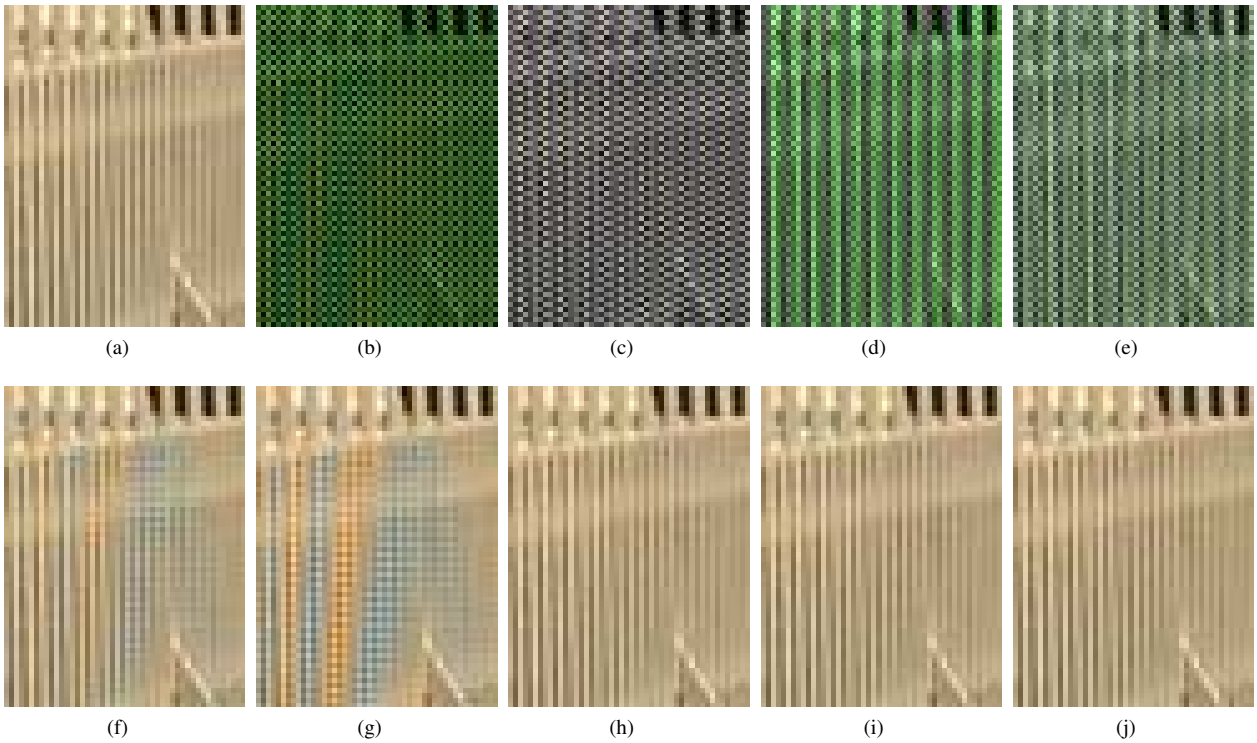

Fig. 4. Top row: (a) Detail of original "lighthouse" image; (b–e) Sensor images using Bayer pattern, pattern I, pattern II, and pattern III, respectively. Bottom row: (f) State-of-the art reconstruction of (b) according to [8]; (g–j) Optimal linear reconstruction of (b–e), respectively.

CFA	Transforms $\mathcal{F}(\boldsymbol{c}_r)$ (top row) and $\mathcal{F}(\boldsymbol{c}_b)$ (bottom row)
I	$\frac{1}{3}\delta(\boldsymbol{\omega}) + \frac{1+i}{12}\delta\left(\boldsymbol{\omega} - \left[\begin{smallmatrix}\pi\\ \frac{\pi}{2}\end{smallmatrix}\right]\right) + \frac{1-i}{12}\delta\left(\boldsymbol{\omega} + \left[\begin{smallmatrix}\pi\\ \frac{\pi}{2}\end{smallmatrix}\right]\right) + \frac{1}{6}\delta\left(\boldsymbol{\omega} - \left[\begin{smallmatrix}\pi\\ \pi\end{smallmatrix}\right]\right)$ $\frac{1}{3}\delta(\boldsymbol{\omega}) + \frac{1+i}{12}\delta\left(\boldsymbol{\omega} - \left[\begin{smallmatrix}\pi\\ \frac{\pi}{2}\end{smallmatrix}\right]\right) + \frac{1-i}{12}\delta\left(\boldsymbol{\omega} + \left[\begin{smallmatrix}\pi\\ \frac{\pi}{2}\end{smallmatrix}\right]\right) - \frac{1}{6}\delta\left(\boldsymbol{\omega} - \left[\begin{smallmatrix}\pi\\ \pi\end{smallmatrix}\right]\right)$
II	$\frac{1}{4}\delta(\boldsymbol{\omega}) + \frac{1+i}{8}\delta\left(\boldsymbol{\omega} - \left[\begin{smallmatrix}\pi\\ \frac{\pi}{2}\end{smallmatrix}\right]\right) + \frac{1-i}{8}\delta\left(\boldsymbol{\omega} + \left[\begin{smallmatrix}\pi\\ \frac{\pi}{2}\end{smallmatrix}\right]\right)$ $\frac{1}{4}\delta(\boldsymbol{\omega}) + \frac{1}{4}\delta\left(\boldsymbol{\omega} - \left[\begin{smallmatrix}\pi\\ \pi\end{smallmatrix}\right]\right)$
III	$\frac{1}{2+\sqrt{2}}\delta(\boldsymbol{\omega}) + \frac{1-i}{4+4\sqrt{2}}\delta\left(\boldsymbol{\omega} - \left[\begin{smallmatrix}\pi\\ \frac{3\pi}{4}\end{smallmatrix}\right]\right) + \frac{1+i}{4+4\sqrt{2}}\delta\left(\boldsymbol{\omega} + \left[\begin{smallmatrix}\pi\\ \frac{3\pi}{4}\end{smallmatrix}\right]\right)$ $\frac{1}{2+\sqrt{2}}\delta(\boldsymbol{\omega}) + \frac{1+i}{4+4\sqrt{2}}\delta\left(\boldsymbol{\omega} - \left[\begin{smallmatrix}\pi\\ \frac{3\pi}{4}\end{smallmatrix}\right]\right) + \frac{1-i}{4+4\sqrt{2}}\delta\left(\boldsymbol{\omega} + \left[\begin{smallmatrix}\pi\\ \frac{3\pi}{4}\end{smallmatrix}\right]\right)$

Table 1. Examples of new color filter array designs based on the method outlined in Section 3. Note that $\boldsymbol{c}_g(\boldsymbol{n}) = 1 - \boldsymbol{c}_r(\boldsymbol{n}) - \boldsymbol{c}_b(\boldsymbol{n})$.

simulated data $\boldsymbol{y}(\boldsymbol{n})$ were obtained for each CFA pattern by "sensing" these test images according to (1). Two contemporary nonlinear demosaicking algorithms [8, 11] were tested in conjunction with the Bayer CFA pattern, and a simple linear demosaicking scheme was employed for each of the three alternative patterns, in which the sensor data were subjected to bandpass filtering in order to recover the modulated difference signals and effect the full-color reconstruction.

A typical example is provided by the "lighthouse" image of Figure 4(a), for which simulated sensor data are shown in Figures 4(b)–4(e), along with their corresponding log-magnitude spectra in Figures 3(e)–3(h). While the Bayer-pattern sensor image of Figure 3(e) indicates aliasing along both the horizontal and vertical axes owing to spectral copies of the difference images $\boldsymbol{\alpha} - \boldsymbol{\beta}$, the frequency-modulated difference images in Figures 3(f)–3(h) have each been shifted well away from the horizontal and vertical axes. Not only does this effect reduce the possibility of aliasing due to horizontal and vertical edges, but it also increases the allowable baseband spectral radius overall, for fixed sensor size relative to the Bayer pattern.

Figures 4(f)–4(j) show reconstructions of the "lighthouse" image. Compared to the nonlinear Bayer demosaicking method of [8] shown in Figure 4(f), as well as to the linear reconstruction shown in Figure 4(g) (whose computational complexity is equal to those of Figures 4(h)–4(j)), the proposed CFAs each yield a marked improvement in visual quality. While we caution that reconstruction results are inevitably a function of the particular demosaicking algorithm employed, and that the test set images cannot provide a true proxy for multi-spectral image data, these results provide encouraging evidence in support of the potential of alternative CFA patterns designed to minimize spatial aliasing and enable simple linear reconstruction schemes. Summary statistics of mean squared error (MSE) measurements shown in Table 2 (averaged over all color channels of the entire 20-image test set) also support this notion; mean and median MSE statistics are improved relative to the state of the art in almost all cases, often by ten percent or more.

5. CONCLUSION

In this paper, we have introduced a new design methodology for CFA patterns in terms of convex combinations of "prototype" color filters whose spectral sensitivities correspond to those of typical red, green, and blue filters in current use. By specifying the desired spatio-spectral response directly in the Fourier domain and providing a corresponding set of optimization criteria, we are able to design patterns that increase the available spatial resolution for fixed sensor size. This design methodology not only sheds light on the failure of simple, linear demosaicking methods in the case of existing color filter arrays such as the well-known Bayer pattern, but also provides for efficient linear demosaicking and a potential for improvements in reconstruction quality for natural images. Our immediate interest is in studying the value of these new patterns to industry from a cost-benefit perspective; to this end future work will include an investigation of noise robustness and performance for various classes of typical images under different illuminants, as well as a careful formulation of meaningful optimality criteria in CFA design overall.

Summary	Bayer CFA		Proposed CFA Patterns		
MSE Statistic	[8]	[11]	I	II	III
Mean	9.97	14.64	8.08	8.99	10.17
Median	8.41	10.99	6.38	7.24	7.65
Minimum	3.99	4.42	2.56	2.77	3.11
Maximum	24.06	47.72	23.11	25.38	36.57
Range	20.07	43.30	20.55	22.61	33.46
Std. Dev.	6.09	11.15	5.20	5.78	7.86

Table 2. Performance comparison for various CFA patterns and reconstruction methods tested on the 20 Kodak test set images of [8].

6. REFERENCES

[1] B. K. Gunturk, J. Glotzbach, Y. Altunbasak, R. W. Schafer, and R. M. Mersereau, "Demosaicking: Color filter array interpolation in single chip digital cameras," *IEEE Signal Process. Mag.*, vol. 22, no. 1, pp. 44–54, Jan. 2005.

[2] B. E. Bayer, "Color imaging array," US Patent 3 971 065, 1976.

[3] R. Lukac and K. N. Plataniotis, "Color filter arrays: Design and performance analysis," *IEEE Trans. Consum. Electron.*, vol. 51, no. 4, pp. 1260–1267, Nov. 2005.

[4] E. Dubois, "Filter design for adaptive frequency-domain Bayer demosaicking," in *Proc. IEEE Internat. Conf. Image Process.*, 2006, pp. 2705–2708.

[5] E. Dubois, "The sampling and reconstruction of time-varying imagery with application in video systems," *Proc. IEEE*, vol. 73, no. 4, pp. 502–522, Apr. 1985.

[6] D. Alleysson, S. Süsstrunk, and J. Hérault, "Linear demosaicing inspired by the human visual system," *IEEE Trans. Image Process.*, vol. 14, no. 4, pp. 439–449, Apr. 2005.

[7] K. Hirakawa, X.-L. Meng, and P. J. Wolfe, "A framework for wavelet-based analysis and processing of color filter array images with applications to denoising and demosaicing," in *Proc. IEEE Internat. Conf. Acoust. Speech Signal Process.*, 2007, vol. 1, pp. 597–600.

[8] B. K. Gunturk, Y. Altunbasak, and R. M. Mersereau, "Color plane interpolation using alternating projections," *IEEE Trans. Image Process.*, vol. 11, no. 9, pp. 997–1013, Sept. 2002.

[9] D. M. Coppola, H. R. Purves, A. N. McCoy, and D. Purves, "The distribution of oriented contours in the real world," *Proc. Natl. Acad. Sci. USA*, vol. 95, pp. 4002–4006, 1998.

[10] N. Zhang and X. Wu, "Lossless compression of color mosaic images," *IEEE Trans. Image Process.*, vol. 15, no. 6, pp. 1379–1388, June 2006.

[11] K. Hirakawa and T. W. Parks, "Adaptive homogeneity-directed demosaicing algorithm," *IEEE Trans. Image Process.*, vol. 14, no. 3, pp. 360–369, Mar. 2005.